Correlation properties of exactly solvable chaotic oscillators

Jonathan N. Blakely and Ned J. Corron
Charles M. Bowden Laboratory, U.S. Army Aviation & Missile Research, Development, & Engineering Center, Redstone Arsenal, Alabama 35898, USA
(Received 9 January 2013; published 12 August 2013)

We derive exact expressions for the autocorrelation and cross-correlation functions of wave forms generated by two exactly solvable chaotic systems. For each system, an analytic expression exists for chaotic solutions, which we use to evaluate correlation integrals explicitly. For some specific parameter values, we calculate the mean and variance of the correlation functions averaged over all possible solutions. The mean autocorrelation is shown to decay at a rate equal to the Kolmogorov-Sinai entropy. All derived results are shown to agree with numerical calculations of the corresponding quantities.

DOI: 10.1103/PhysRevE.88.022909 PACS number(s): 05.45.Ac, 02.90.+p

I. INTRODUCTION

Conventional wisdom holds that chaotic dynamical systems cannot be solved analytically. Although there have always been exceptions to this rule, a class of discontinuous differential equations has recently been shown to have exact chaotic solutions that can be written in a particularly simple form, i.e., a convolution of a single basis function with a train of regularly timed, random binary amplitudes [1,2]. Physical implementations of these systems include electronic circuits and electromechanical oscillators [1,3–7]. These solvable systems are of fundamental scientific interest because they can be analyzed with an unusual degree of rigor. For example, in at least two cases, an exact topological conjugacy between a solvable system and the Bernoulli shift map has been identified, which constitutes rigorous proof of chaos [1,2]. The same cannot be said for such paradigms of nonlinear dynamics as the Lorenz and Rossler systems [8,9]. Moreover, statistical properties such as Lyapunov exponents, fractal dimension, and metric entropy, which are typically estimated by lengthy numerical analysis, can be determined exactly for these systems. Solvable systems are of practical interest in applications for the very same reason. Technologies based on these oscillators can be analyzed more thoroughly than those based on better known chaotic oscillators. For example, exact expressions have been derived for bit error rates in communication schemes that use solutions of solvable chaotic systems as communication wave forms [1,10,11]. In addition, detailed knowledge of the wave form allows for the design of simple yet optimal receivers for communication and radar [1,11–14].

Here we exploit the analytic solutions of two solvable systems to determine exactly the correlation properties of the chaotic oscillations. In general, the correlation properties of a system reveal important aspects of its dynamics, such as the degree to which the system can be treated as stochastic versus deterministic [15], or the degree to which the system interacts with others [16]. Chaotic oscillations typically display large short-time correlations followed by exponentially decaying long-term correlations, a phenomenon known as correlation splitting that is related to mixing [17]. In contrast, intermittent dynamics are characterized by power law correlation decay [18–20]. In analyzing experimental data, correlations are often more easily estimated than other properties such as Lyapunov exponents or fractal dimension. Finally, correlation properties are often directly relevant to performance of technologies based on chaos. For example, in a chaos-based random number generator correlations determine the amount of postprocessing necessary to extract truly random bits [21,22]. In a chaotic radar system, the autocorrelation function of the transmitted wave form determines the range resolution and ambiguity, while cross correlations with other wave forms determine the ability of multiple users to operate simultaneously [23,24]. In digital watermarking with chaotic sequences, correlation is used as a test statistic to distinguish a watermarked image from an unmarked image [25]. Many studies of correlations in chaotic systems can be found in the literature. Most significant theoretical progress has been made with regard to a class of systems known as Anosov flows [15,17,26–34]. However, it is quite rare to find results as explicit as those we present here.

In Sec. II, we introduce two solvable chaotic dynamical systems and give their analytic solutions. In Sec. III, we derive an exact expression for the autocorrelation of wave forms generated by these oscillators, and in Sec. IV, we do the same for the cross correlation. In Sec. V, we show that at certain parameter values, exact expressions can be derived for statistics of the autocorrelation and the cross correlation averaged over the ensemble of all possible solutions. In one case, the mean autocorrelation is shown to decay at a rate equal to the Kolmogorov-Sinai entropy. Finally, in Sec. VI we discuss the significance of these results for some potential technological applications.

II. EXACTLY SOLVABLE CHAOTIC OSCILLATORS

Here we introduce two examples of chaotic dynamical systems for which an exact solution is known. Both oscillators are hybrid dynamical systems defined by a differential equation along with a guard condition as follows. For both oscillators, the differential equation is the linear, second order equation,

$$\frac{d^2u}{dt^2} - 2\beta\frac{du}{dt} + (\omega^2 + \beta^2)(u - s) = 0, \tag{1}$$

where $u(t)$ is a continuous state variable and $s(t)$ is a discrete state. In experimental implementations, $u(t)$ may represent a voltage across a capacitor [1,3–6] or a mass on a spring [7]. Throughout this paper, we fix $\omega = 2\pi$ in order to conveniently

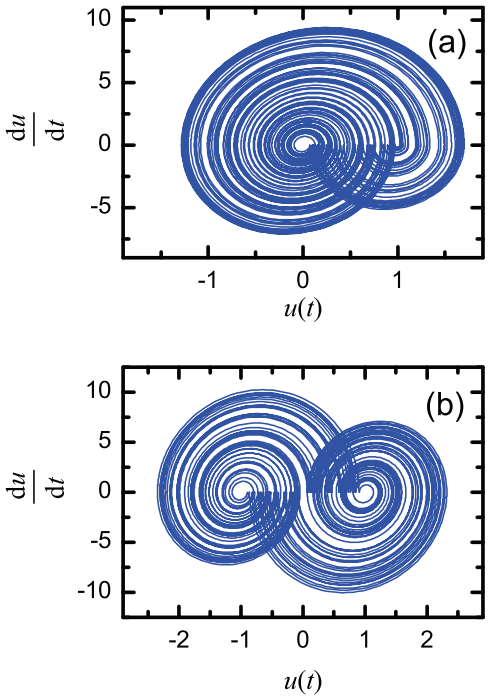

FIG. 1. (Color online) Phase projections of typical trajectories of the (a) exact folded-band oscillator with $\beta = 0.81 \times \ln 2$ and (b) exact shift oscillator with $\beta = \ln 2$.

scale time. In addition, β is a positive constant whose value will be discussed further below.

The discrete state $s(t)$ is updated when a guard condition is satisfied. The choice of guard condition distinguishes between the two oscillators considered here. First, a Rossler-like oscillation results from the condition,

$$\frac{du}{dt} = 0 \quad \Rightarrow \quad s(t) = H(u(t) - 1), \tag{2}$$

meaning whenever the derivative of $u(t)$ vanishes the discrete state $s(t)$ is set to $H(u(t) - 1)$, where $H(x)$ is the left-continuous Heaviside function. The state $s(t)$ maintains this value until the guard condition is next met. A phase projection of a typical trajectory of this hybrid system is shown in Fig. 1(a). Due to the Rossler-like, folded-band topology of this orbit, we refer to this system as the *exact folded-band oscillator* [2].

For a chaotic solution valid for all t that passes through the point $u(0) = u_0$, $du/dt(0) = 0$, and $s(0) = H(u_0 - 1)$ for some u_0, the continuous state $u(t)$ can be expressed by the infinite sum,

$$u(t) = \sum_{m=-\infty}^{\infty} \sigma_m Q(t - \frac{m}{2}), \tag{3}$$

where each term is a basis pulse of shape $Q(t)$ defined as

$$Q(t) = \begin{cases} Q_1(t), & t < 0 \\ Q_2(t), & 0 \leqslant t \leqslant \frac{1}{2} \\ 0, & \frac{1}{2} \leqslant t \end{cases}, \tag{4}$$

where

$$Q_1(t) = (1 + e^{-\beta/2})e^{\beta t}\left(\cos \omega t - \frac{\beta}{\omega} \sin \omega t\right), \tag{5}$$

and

$$Q_2(t) = 1 + e^{\beta(t-1/2)}\left(\cos \omega t - \frac{\beta}{\omega} \sin \omega t\right). \tag{6}$$

Each pulse is weighted by a coefficient σ_m, the value of which is either 1 or 0.

A topologically distinct oscillation results from the guard condition,

$$\frac{du}{dt} = 0 \quad \Rightarrow \quad s(t) = \mathrm{sgn}(u(t)), \tag{7}$$

meaning the discrete state $s(t)$ is set to the sign of $u(t)$ whenever the derivative of $u(t)$ vanishes. A phase projection of a typical trajectory of this system is shown in Fig. 1(b). This system displays a return map which is a shift map; therefore, we refer to this system as the *exact shift oscillator* [1].

For a chaotic solution valid for all t that passes through the point $u(0) = u_0$, $du/dt(0) = 0$, and $s(0) = \mathrm{sgn}(u_0)$ for some u_0, the continuous state $u(t)$ can be expressed by the infinite sum,

$$u(t) = \sum_{m=-\infty}^{\infty} \sigma_m P(t - m), \tag{8}$$

where the basis pulses in this case are

$$P(t) = Q(t) + Q\left(t - \tfrac{1}{2}\right), \tag{9}$$

and each coefficient σ_m is either $+1$ or -1.

III. AUTOCORRELATION

The autocorrelation of a wave form $u(t)$ is typically defined as

$$R(\tau) = \lim_{T\to\infty} \frac{1}{T} \int_{-T/2}^{T/2} u(t)u(t + \tau)dt, \tag{10}$$

where τ is a lag parameter [35]. The value of R at $\tau = 0$ is interpreted as the average signal power. Due to the structure of the wave forms of interest here, we introduce an alternative, but equivalent limit to define the correlation. First, note that for these solvable oscillators, a finite segment of a solution of the form of Eqs. (3) and (8) containing $2N + 1$ terms can be expressed as

$$u_N(t) = \sum_{m=-N}^{N} \sigma_m F(t - mT_0), \tag{11}$$

where F is the appropriate basis pulse, and T_0 is the period between pulses, or *pulse spacing*. Then we define autocorrelation as

$$R(\tau) = \lim_{N\to\infty} \frac{1}{(2N + 1)T_0} \int_{-\infty}^{\infty} u_N(t)u_N(t + \tau)dt. \tag{12}$$

As with the conventional definition for R, the value at zero lag gives the average signal power. Substituting Eq. (11) into

Eq. (12) gives the expression,

$$R(\tau) = \lim_{N\to\infty} \sum_{m=-N}^{N} \sum_{n=-N}^{N} \frac{\sigma_m \sigma_n K(mT_0 - nT_0 + \tau)}{(2N+1)T_0}, \tag{13}$$

where

$$K(\tau) = \int_{-\infty}^{\infty} F(t)F(t+\tau)dt \tag{14}$$

is the overlap integral for two displaced instances of the basis pulse function $F(t)$. Thus, calculation of the autocorrelation is reduced to evaluation of overlap integrals of the corresponding basis pulse.

For the exact folded-band oscillator, $F(t) = Q(t)$ and $T_0 = 1/2$, so Eq. (13) gives the autocorrelation as

$$R(\tau) = \lim_{N\to\infty} \sum_{m=-N}^{N} \sum_{n=-N}^{N} \frac{2\sigma_m \sigma_n J\left(\frac{m}{2} - \frac{n}{2} + \tau\right)}{2N+1}, \tag{15}$$

where

$$J(\tau) = \int_{-\infty}^{\infty} Q(t)Q(t+\tau)dt \tag{16}$$

is the overlap integral for two instances of the basis pulse function $Q(t)$ displaced by a lag τ. For $0 < \tau < 1/2$, using Eq. (4), this integral can be expressed as

$$J(\tau) = \int_{-\infty}^{-\tau} Q_1(t)Q_1(t+\tau)dt + \int_{-\tau}^{0} Q_1(t)Q_2(t+\tau)dt + \int_{0}^{\frac{1}{2}-\tau} Q_2(t)Q_2(t+\tau)dt, \tag{17}$$

while for $\tau > 1/2$,

$$J(\tau) = \int_{-\infty}^{-\tau} Q_1(t)Q_1(t+\tau)dt + \int_{-\tau}^{\frac{1}{2}-\tau} Q_1(t)Q_2(t+\tau)dt. \tag{18}$$

In these expressions, the integrals should be interpreted as having zero value if the lower limit exceeds the upper limit. Explicit expressions for these integrals are

$$\int_{-\infty}^{-\tau} Q_1(t)Q_1(t+\tau)dt = \frac{(1+e^{-\beta/2})^2 e^{-\beta\tau}}{4(\beta^2+\omega^2)} \left\{ \left(\frac{\omega^2}{\beta} + 5\beta\right)\cos(\omega\tau) + \left(\frac{3\beta^2}{\omega} - \omega\right)\sin(\omega\tau) \right\}, \tag{19}$$

$$\int_{-\tau}^{0} Q_1(t)Q_2(t+\tau)dt = \frac{(1+e^{-\beta/2})e^{-\beta\tau}}{\beta^2+\omega^2} \left\{ 2\beta e^{\beta\tau} + \left[\left(\frac{\omega^2}{4\beta} + \frac{5\beta}{4}\right)(e^{\beta(2\tau-1/2)} - e^{-\beta/2}) - 2\beta \right]\cos(\omega\tau) + \left[\left(\frac{\omega}{4} - \frac{3\beta^2}{4\omega}\right)(e^{\beta(2\tau-1/2)} + e^{-\beta/2}) + \omega - \frac{\beta^2}{\omega} \right]\sin(\omega\tau) \right\}, \tag{20}$$

$$\int_{0}^{\frac{1}{2}-\tau} Q_2(t)Q_2(t+\tau)dt = \frac{1}{2} - \tau + \frac{e^{\beta(\tau-1)}}{\beta^2+\omega^2} \left\{ -2\beta\left(e^{\beta(1-\tau)} + e^{\beta(\frac{1}{2}-\tau)}\right) + \left[\left(\frac{3\omega}{4} - \frac{\beta^2}{4\omega}\right)e^{\beta(1-2\tau)} - \left(\omega - \frac{\beta^2}{\omega}\right)e^{\frac{\beta}{2}} + \frac{3\beta^2}{4\omega} - \frac{\omega}{4} \right]\sin(\omega\tau) + \left[\left(\frac{\omega^2}{4\beta} - \frac{3\beta}{4}\right)e^{\beta(1-2\tau)} - 2\beta e^{\beta/2} - \frac{\omega^2}{4\beta} - \frac{5\beta}{4} \right]\cos(\omega\tau) \right\}, \tag{21}$$

and

$$\int_{-\tau}^{\frac{1}{2}-\tau} Q_1(t)Q_2(t+\tau)dt = \frac{(1+e^{-\beta/2})e^{-\beta\tau}}{\beta^2+\omega^2} \left\{ \left[\left(\frac{\omega^2}{4\beta} - \frac{3\beta}{4} + \frac{\beta^3-\beta^2}{4\omega^2}\right)e^{\beta/2} - \left(\frac{5\beta}{4} + \frac{\omega^2}{4\beta}\right)e^{-\beta/2} - 2\beta \right]\cos(\omega\tau) + \left[\left(\frac{3\omega}{4} - \frac{\beta^2}{4\omega}\right)e^{\beta/2} + \left(\frac{\omega}{4} - \frac{3\beta^2}{4\omega}\right)e^{-\beta/2} + \omega - \frac{\beta^2}{\omega} \right]\sin(\omega\tau) \right\}. \tag{22}$$

Altogether, these results provide an explicit expression for the autocorrelation function of a folded-band oscillation of the form of Eq. (3).

Figure 2 shows an example illustrating our results for the exact folded-band oscillator with $\beta = 0.81 \times \ln 2$. In Fig. 2(a), a truncated wave form of the form of Eq. (11), with $N = 50$, is shown. In Fig. 2(b), the autocorrelation function given by Eq. (15) is plotted. The explicit expression was verified by the numerical quadrature of Eq. (12). The numerical result coincided with the analytical result to such a degree that the two are indistinguishable on the scale of the figure. The autocorrelation function in this example displays the expected large peak at $\tau = 0$, along with small fluctuations at larger lags dependent on the detailed shape of the particular oscillation chosen.

For the exact shift oscillator, $F(t) = P(t)$ and $T_0 = 1$, so the autocorrelation is

$$R(\tau) = \lim_{N\to\infty} \sum_{m=-N}^{N} \sum_{n=-N}^{N} \frac{\sigma_m \sigma_n I(m-n+\tau)}{2N+1}, \tag{23}$$

where

$$I(\tau) = \int_{-\infty}^{\infty} P(t)P(t+\tau)dt \tag{24}$$

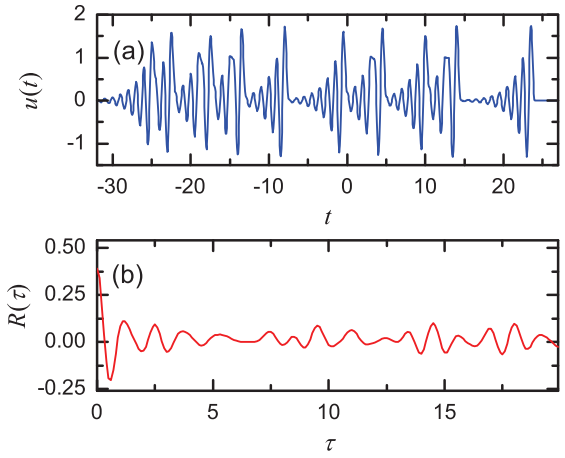

FIG. 2. (Color online) (a) A randomly selected wave form of the exact folded-band oscillator with $\beta = 0.81 \times \ln 2$, truncated with $N = 50$. (b) The autocorrelation for the wave form in (a) given by Eq. (13).

is the overlap integral for basis functions of the shift oscillator. Using Eq. (9) it can be shown that

$$I(\tau) = 2J(\tau) + J(\tau - 1/2) + J(\tau + 1/2). \tag{25}$$

A typical autocorrelation function for the exact shift oscillator is shown in Fig. 3. A wave form truncated with $N = 50$ is shown in Fig. 3(a). The autocorrelation given by Eq. (23) for this wave form is shown in Fig. 3(b). A quantitative difference is apparent between these results and those for the exact folded band. Note the peak at zero lag is more prominent than in the folded-band case. This peak is larger because the exact shift oscillator has a basis pulse at every integer time step. Thus the average power is roughly equal to the energy of one bit per unit time. In contrast, in a folded-band wave form basis pulses may or may not be present at each half-integer time. So the average power is less than the energy of one pulse per half time unit.

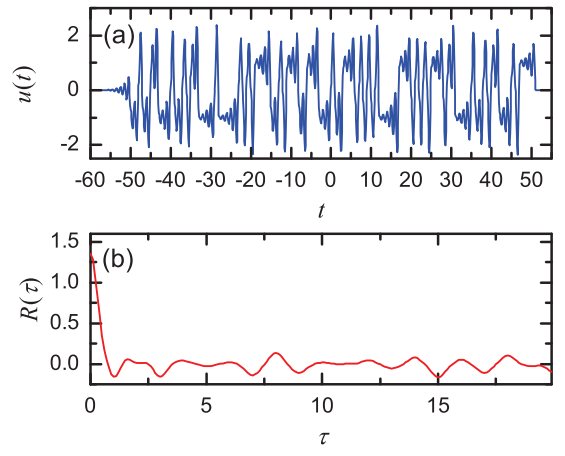

FIG. 3. (Color online) (a) A randomly selected wave form of the exact shift oscillator with $\beta = \ln 2$, truncated with $N = 50$. (b) The autocorrelation for the wave form in (a) given by Eq. (23).

IV. CROSS CORRELATION

The definition of cross correlation follows predictably from that of autocorrelation as

$$C(\tau) = \lim_{T\to\infty} \frac{1}{T} \int_{-T/2}^{T/2} u(t)u'(t+\tau)dt, \tag{26}$$

where $u(t)$ and $u'(t)$ are distinct wave forms. As we did for the autocorrelation, we introduce an equivalent definition of cross correlation that can be evaluated exactly, i.e.,

$$C(\tau) = \lim_{N\to\infty} \frac{1}{NT_0} \int_{-\infty}^{\infty} u_N(t)u'_N(t+\tau)dt, \tag{27}$$

where $u_N(t)$ and $u'_N(t)$ are two wave forms from the same solvable chaotic system and defined analogously to Eq. (11). For such wave forms, this expression becomes

$$C(\tau) = \lim_{N\to\infty} \sum_{m=-N}^{N} \sum_{n=-N}^{N} \frac{\sigma_m \sigma'_n K(mT_0 - nT_0 + \tau)}{(2N+1)T_0}, \tag{28}$$

where σ_m is the m^{th} coefficient of the wave form u_N, σ'_n is the n^{th} coefficient of the wave form u'_N, and K is the overlap integral of the appropriate basis pulse.

For two wave forms of the exact folded-band oscillator, Eq. (28) gives the cross correlation as

$$C(\tau) = \lim_{N\to\infty} \sum_{m=-N}^{N} \sum_{n=-N}^{N} \frac{2\sigma_m \sigma'_n J\left(\frac{m}{2} - \frac{n}{2} + \tau\right)}{(2N+1)}. \tag{29}$$

Two such wave forms, each with $N = 50$, are shown in Figs. 4(a) and 4(b). Their cross correlation is shown in Fig. 4(c) given by Eq. (29). Typical of folded-band wave forms, the cross correlation in this case has a periodicity corresponding to the two wave forms coming in and out of phase as the lag increases.

For wave forms of the exact shift oscillator, the cross correlation is given by

$$C(\tau) = \lim_{N\to\infty} \sum_{m=-N}^{N} \sum_{n=-N}^{N} \frac{\sigma_m \sigma'_n I(m - n + \tau)}{2N+1}. \tag{30}$$

Two such wave forms, each with $N = 50$, are shown in Figs. 5(a) and 5(b). Their cross correlation, given by Eq. (30), is shown in Fig. 5(c). In contrast with the folded-band case, no periodicity is apparent, consistent with the lack of a monotonically increasing phase in the chaotic set of Fig. 1(b).

V. STATISTICAL PROPERTIES OF CORRELATIONS

The correlation functions of the preceding sections characterize individual wave forms of each solvable system. It is often of interest to determine statistical properties of correlation functions for a dynamical system, as well. Such properties are derived from averaging over the ensemble of all possible wave forms a single oscillator can produce, properly weighted by the natural invariant density. In general, it is not easy to express the natural invariant density of a chaotic oscillator exactly. However, for some specific values of β, the solvable systems of interest here have uniform natural invariant densities allowing

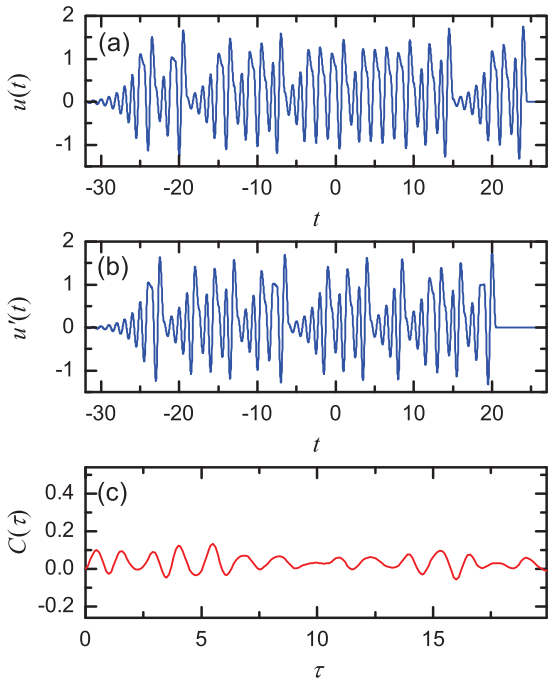

FIG. 4. (Color online) Randomly selected wave forms [(a) and (b)] of the exact folded-band oscillator with $\beta = 0.81 \times \ln 2$ truncated with $N = 50$. (c) Cross correlation for these wave forms given by Eq. (28).

for exact determination of the ensemble average properties of the wave forms they generate. In this section, we derive the mean and variance of the correlation functions for the exact shift and exact folded-band oscillators with specific parameter values.

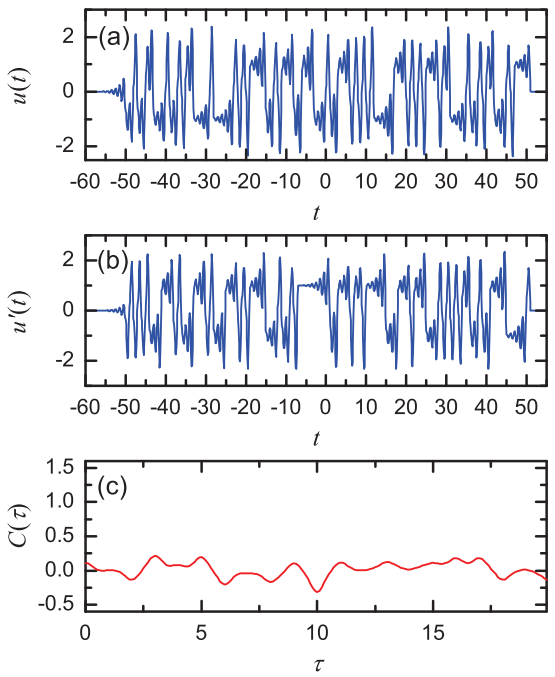

FIG. 5. (Color online) Randomly selected wave forms [(a) and (b)] of the exact shift oscillator with $\beta = \ln 2$ truncated with $N = 50$. (c) Cross correlation for these wave forms given by Eq. (30).

A. Statistical properties of the exact shift oscillator

For the exact shift oscillator with $\beta = \ln 2$ a return map based on samples at integer times is the Bernoulli shift map [1]. This map has a uniform invariant density over the interval $[0,1]$ and a Markov partition at $1/2$. The σ_m coefficients in Eq. (8) directly correspond to the symbol sequences generated by this Markov map. Thus, we can conclude that for solutions of the form of Eq. (8), the sequence of coefficients σ_m can be any infinite sequence of $+1$'s and -1's, and every sequence is equally likely. Equivalently, we can say that the coefficients are independent random variables with equal probability of being a $+1$ or a -1, so that

$$\langle \sigma_m \sigma_n \rangle = \delta_{mn}, \tag{31}$$

and

$$\langle \sigma_k \sigma_l \sigma_m \sigma_n \rangle = \delta_{mn}\delta_{kl} + \delta_{lm}\delta_{kn} + \delta_{ln}\delta_{km} - 2\delta_{klmn}, \tag{32}$$

for any non-negative integers k, l, m, and n. Here the angle brackets signify an average over all possible chaotic solutions of the exact shift oscillator, δ_{mn} is the Kronecker delta function, and δ_{klmn} is equal to 1 if and only if $k = l = m = n$, and is 0 otherwise. Using this information, we can determine the ensemble mean autocorrelation function to be

$$\langle R(\tau) \rangle = \lim_{N\to\infty} \sum_{m=-N}^{N} \sum_{n=-N}^{N} \frac{\langle \sigma_m \sigma_n \rangle I(m-n+\tau)}{2N+1} = I(\tau). \tag{33}$$

In Fig. 6(a), $\langle R(\tau) \rangle$, given by Eq. (33), is plotted (solid red line) along with the numerical estimate of $\langle R(\tau) \rangle$ (dashed blue line) derived from an ensemble of 100 randomly generated wave forms. The sample wave forms are truncated with $N = 50$. Apparent in the figure is the phenomenon of correlation splitting where the mean correlation function has a peak at zero followed by an exponentially decaying oscillatory tail. Decaying long-term correlations are known to be a consequence of mixing in a dynamical system. Typically, for

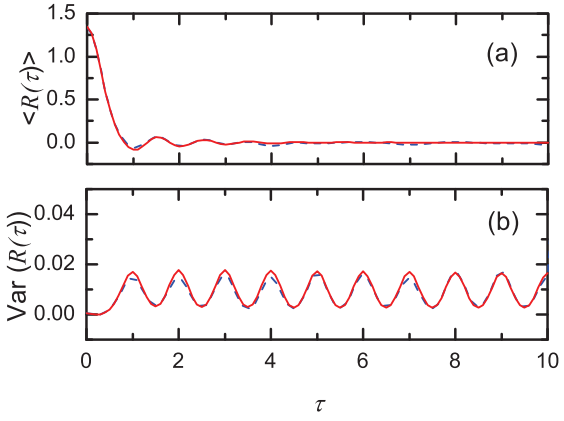

FIG. 6. (Color online) Statistical properties of the autocorrelation function of wave forms of the exact shift oscillator of length $N = 100$. (a) Mean value of the autocorrelation function estimated numerically (dashed blue line) from a sample of 100 wave forms, and calculated exactly (solid red line). (b) Variance of the autocorrelation function estimated numerically (dashed blue line), and calculated exactly (solid red line).

chaotic systems it has been observed that the tail of the mean autocorrelation function lies within an envelope that decays exponentially [36].

Through Eq. (33) the correlation splitting can be viewed as a direct consequence of the shape of the overlap integral [Eq. (24)]. Specifically, for $\tau < 1$, $I(\tau)$ contains terms of the form of Eqs. (21) and (22) which do not decay with increasing τ. In contrast, for $\tau > 1$, $I(\tau)$ contains only terms of the form of Eqs. (19) and (23), both of which take the form of an oscillatory amplitude multiplied by a factor $e^{-\beta\tau}$. We can immediately conclude that $\langle R(\tau)\rangle$ decays at a rate equal to $\beta = \ln 2$, which is exactly the value of the Kolmogorov-Sinai entropy, as follows from the full shift in the symbolic dynamics of the system [1].

Using Eq. (32), the variance of the autocorrelation can be determined to be

$$\begin{aligned}\mathrm{Var}(R(\tau)) &= \langle R(\tau)^2\rangle - \langle R(\tau)\rangle^2 \\ &= \lim_{N\to\infty}\frac{1}{(2N+1)^2} \\ &\quad\times \sum_{m=-N}^{N}\sum_{n=-N}^{N} I(m-n+\tau)\{I(n-m+\tau) \\ &\quad + I(m-n+\tau)\} - \lim_{N\to\infty} 2\frac{I(\tau)^2}{(2N+1)}. \end{aligned} \tag{34}$$

The last term vanishes in the limit as N goes to infinity, but must be retained in any approximation using finite length wave forms. In Fig. 6(b), the theoretical variance is plotted (solid red line) along with the numerically estimated variance of the autocorrelation (dashed blue line) derived from the ensemble of 100 randomly generated wave forms mentioned earlier.

Similar reasoning can be used to find the statistical properties of the cross correlation, as well. Assuming we have two solutions $u(t)$ and $u'(t)$ with coefficients σ_m and σ'_m, respectively, then

$$\langle \sigma_m \sigma'_n\rangle = 0, \tag{35}$$

and

$$\langle \sigma_k \sigma'_l \sigma_m \sigma'_n\rangle = \delta_{km}\delta_{ln}. \tag{36}$$

The mean value of the cross correlation is

$$\begin{aligned}\langle C(\tau)\rangle &= \lim_{N\to\infty}\sum_{m=-N}^{N}\sum_{n=-N}^{N}\frac{\langle\sigma_m\sigma'_n\rangle I(m-n+\tau)}{2N+1} \\ &= 0. \end{aligned} \tag{37}$$

The variance is

$$\mathrm{Var}(C(\tau)) = \lim_{N\to\infty}\sum_{m=-N}^{N}\sum_{n=-N}^{N}\frac{I(m-n+\tau)^2}{(2N+1)^2}. \tag{38}$$

These results compare well to numerical estimates of the same quantities based on an ensemble of 100 wave forms with $N = 50$. In Fig. 7(a), the vanishing of the mean predicted by Eq. (37) (red line) agrees with the numerically estimated mean cross correlation (blue line). A vanishing cross-correlation function can be interpreted as a kind of statistical orthogonality

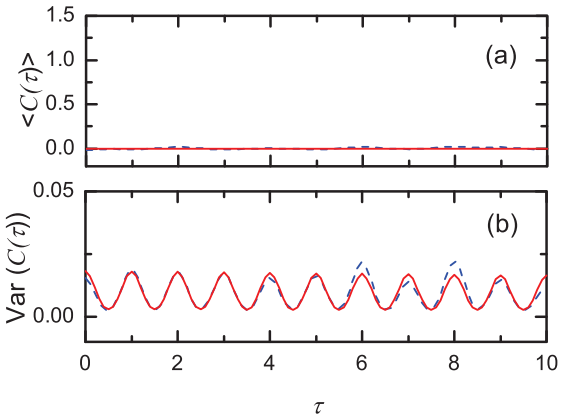

FIG. 7. (Color online) Statistical properties of the cross-correlation function of wave forms of the exact shift oscillator of length $N = 50$. (a) Mean value of the cross-correlation function estimated numerically (dashed blue line) from a sample of 100 wave forms, and calculated exactly (solid red line). (b) Variance of the cross-correlation function estimated numerically (dashed blue line), and calculated exactly (solid red line).

that is often a significant advantage in signal processing [35]. In Fig. 7(b), the periodic oscillation of the variance given by Eq. (38) (red line) agrees with the numerically estimated variance (blue line).

B. Statistical properties of the exact folded-band oscillator

For the exact folded-band oscillator with $\beta = \beta_1$ where β_1 satisfies the equation,

$$e^{\beta_1} = 1 + e^{-\beta_1/2}, \tag{39}$$

the peak return map is a skewed tent map on the interval $[0, e^{\beta_1}]$ [2]. The numerical value of β_1 is approximately $0.81 \times \ln 2$. This map has a uniform invariant density over $[0, e^{\beta_1}]$, and a Markov partition at 1. The partition separates the region $[0,1)$, with which we associate the symbol A, from the region $(1, e^{\beta_1}]$, with which we associate the symbol B. Together, the uniform density and the Markov property imply that each symbol generated by the return map is an independent random variable with the probability of an A being generated as

$$p(A) = e^{-\beta_1}, \tag{40}$$

and the probability of a B,

$$p(B) = 1 - e^{-\beta_1}. \tag{41}$$

In contrast to the case of the exact shift oscillator, the returns of this map do not have a single fixed return time. So the σ_m coefficients in Eq. (3) do not directly correspond to the symbol sequences generated by the return map. However, it has been shown that the following correspondence does hold:

$$A \to 00, \quad B \to 100. \tag{42}$$

Thus, beginning with a sequence of As and Bs generated using the probabilities of Eqs. (40) and (41), we can construct a sequence of σ_m coefficients that corresponds to a randomly selected valid solution of the exact folded-band oscillator. For such sequences, the probability of any given σ_m coefficient

being equal to 1 is

$$p(1) = \frac{1 - e^{-\beta_1}}{3 - e^{-\beta_1}}. \tag{43}$$

However, unlike the A and B symbols, the σ_m coefficients are correlated due to the grammar imposed by Eq. (42).

These correlations must be taken into account in determining $\langle \sigma_m \sigma_n \rangle$. The trivial case where $n = m$ is simply

$$\langle \sigma_m \sigma_m \rangle = p(1). \tag{44}$$

For some integer $k \geqslant 3$,

$$\langle \sigma_m \sigma_{m\pm k} \rangle = p(1) \times \sum_i p(\{\sigma_1, \ldots, \sigma_{k-3}\}_i) p(B), \tag{45}$$

where $\{\sigma_1, \sigma_2, \ldots, \sigma_{k-3}\}_i$ is the i^{th} distinct sequence of length $k-3$, and the sum gives the total probability for all sequences of length $k-3$. This expression follows from recognizing that a product of the form $\sigma_m \sigma_{m\pm k}$ can only be nonzero if both σ_m and $\sigma_{m\pm k}$ are nonzero, which requires both to be derived from B symbols. There is only a finite number of sequences of a given length that can fit between two B symbols. These can be constructed systematically using Eq. (42), and assigned probabilities using Eqs. (40) and (41) as detailed in the appendix. The mean autocorrelation is then

$$\langle R(\tau) \rangle = \lim_{N\to\infty} \sum_{m=-N}^{N} \sum_{n=-N}^{N} \frac{2\langle \sigma_m \sigma_n \rangle J\left(\frac{m}{2} - \frac{n}{2} - \tau\right)}{2N+1}. \tag{46}$$

The function $\langle R(\tau) \rangle$ given by Eq. (46) is shown in Fig. 8 (solid red line) along with a numerical estimate (dashed blue line) of the mean autocorrelation derived from an ensemble of 100 wave forms with $N = 50$. As was the case with the exact shift oscillator, correlation splitting can be seen and directly connected to the exponential tails of the overlap integrals $J(\tau)$.

Following similar reasoning, an expression for the variance of the autocorrelation can also be derived. Unfortunately, due to the correlations between the σ_m coefficients, the resulting expression is quite cumbersome and impractical. Therefore, we omit it here.

The mean and variance of the cross correlation are much simpler to derive since there are no correlations between the σ_m coefficients of two separate wave forms. Assuming we have two solutions $u(t)$ and $u'(t)$ with coefficients σ_m and σ'_m, respectively, then

$$\langle \sigma_m \sigma'_n \rangle = p(1)^2, \tag{47}$$

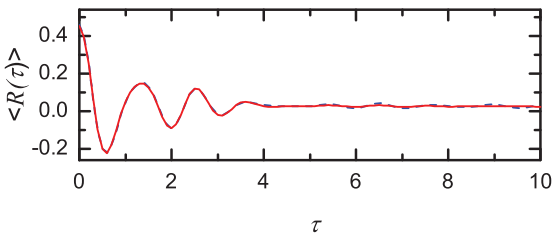

FIG. 8. (Color online) Mean value of the autocorrelation function for wave forms of the exact folded-band oscillator with $N = 50$ estimated numerically (dashed blue line) from a sample of 100 wave forms, and calculated exactly (solid red line).

and

$$\langle \sigma_k \sigma'_l \sigma_m \sigma'_n \rangle = p(1)^2 p(B)^2 \sum_i p(\{\sigma_1, \ldots, \sigma_{|k-m|-3}\}_i) \times \sum_j p(\{\sigma_1, \ldots, \sigma_{|l-n|-3}\}_j), \tag{48}$$

where the first sum gives the total probability for all sequences of length $|k-m|-3$, and the second sum gives the total probability for all sequences of length $|l-n|-3$.

It follows immediately that

$$\langle C(\tau) \rangle = \lim_{N\to\infty} \sum_{m=-N}^{N} \sum_{n=-N}^{N} \frac{2p(1)^2 J\left(\frac{m}{2} - \frac{n}{2} - \tau\right)}{2N+1}, \tag{49}$$

and

$$\mathrm{Var}(C(\tau)) = \lim_{N\to\infty} \sum_{k=-N}^{N} \sum_{l=-N}^{N} \sum_{m=-N}^{N} \sum_{n=-N}^{N} \times \frac{4\{\langle \sigma_k \sigma'_l \sigma_m \sigma'_n \rangle - p(1)^4\} J\left(\frac{k}{2} - \frac{l}{2} - \tau\right) J\left(\frac{m}{2} - \frac{n}{2} - \tau\right)}{(2N+1)^2}. \tag{50}$$

Again, these expressions are verified by comparison to numerical estimates of the mean and variance. The function $\langle C(\tau) \rangle$ is shown in Fig. 9(a) along with a numerical estimate of the mean derived from an ensemble of 100 wave forms with $N = 50$. Notably, the mean cross correlation appears to have a constant, nonzero value. This property can be attributed to the nonzero mean of the folded-band wave forms. The same value is approached by the mean autocorrelation given by Eq. (46) for large lags where the correlations between the σ_m coefficients are negligible. The variance given by Eq. (50) is shown in Fig. 9(b) along with a numerical estimate which agrees closely.

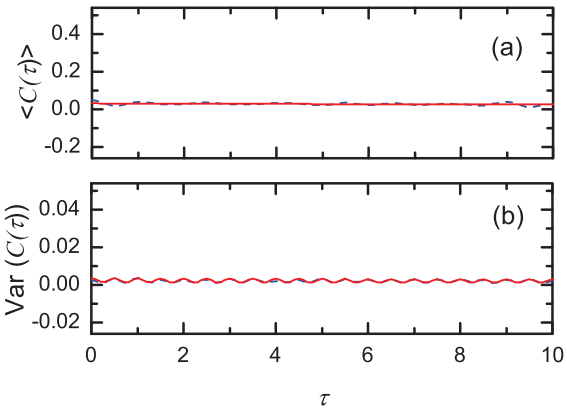

FIG. 9. (Color online) Statistical properties of the cross-correlation function of wave forms of the exact folded-band oscillator with $N = 50$. (a) Mean value of the cross-correlation function estimated numerically (dashed blue line) from a sample of 100 wave forms, and calculated exactly (solid red line). (b) Variance of the cross-correlation function estimated numerically (dashed blue line), and calculated exactly (solid red line).

VI. CONCLUSION

In this paper, we derived exact formulas for correlation functions of wave forms of the exact folded-band oscillator and the exact shift oscillator. We first showed that evaluation of the autocorrelation and cross-correlation functions for specific wave forms could be reduced to evaluating overlap integrals for the appropriate basis pulse of each oscillator. Next, we showed that for specific parameter values, average properties of these functions could be calculated exactly as well. Both the mean and variance of the autocorrelation and cross-correlation functions were derived. Observed correlation splitting was shown to be a result of the decaying tail of the basis function overlap integral.

These results have direct practical consequences for applications of these solvable chaotic oscillators. For example, consider a radar based on these chaotic systems. In such a system, an electronic oscillator outputs a voltage that is the solution of a solvable chaotic system to be used as the transmitted wave form. The half-width of the mean autocorrelation functions provides a measure of the range resolution these wave forms could achieve in a radar system. In the case of the exact shift oscillator, the half-width is approximately 0.37, in time units scaled to make the pulse repetition rate equal 1. For an oscillator circuit with a pulse repetition rate of 100 MHz emitting radio waves, the width of the autocorrelation would be 3.7 ns, corresponding to a range resolution of 3.7 ns $\times$ 3 $\times 10^8$m/s $= 1.1$ m. On the other hand, the width of the mean autocorrelation for the folded-band oscillator is approximately 0.21, in time units scaled to make the pulse repetition rate equal 1/2. For an electronic folded-band oscillator with a pulse repetition rate of 100 MHz, the range resolution would be 1.3 m, slightly larger than that of the shift oscillator. As another example consider the vanishing of the mean cross correlation for the exact shift oscillator. This statistical orthogonality enables the use of multiple chaotic radars in close proximity without significant interference.

An important area for future work is the search for other solvable chaotic systems. For example, perhaps solvable oscillators with chaotic sets of distinct topologies may be found. Perhaps a solvable delay dynamical system is possible. If so, it is reasonable to expect the wave forms of such systems would be of the form of Eqs. (3) and (8), in which case the correlation functions could be determined exactly through derivations along the lines of those presented here.

APPENDIX

As a result of the coding in Eq. (42), for any positive integer $k > 3$, a symbol sequence (made up of As and Bs) corresponding to a sequence of $k-3$ coefficients (i.e., 1s and 0s) must satisfy the equation,

$$2m + 3n = k - 3, \tag{A1}$$

where m is the number of As in the symbol sequence and n is the number of Bs. The value of n for any solution must be a member of the set of integers from zero to $(k-3)/3$. Any value in this range gives a solution $(m = (k-3-3n)/2, n)$ if and only if $(k-3-3n)/2$ is a whole number. The potential values of n can be checked sequentially. For a given solution (m,n), there are $(m+n)!/(m!+n!)$ sequences including all possible permutations of the As and Bs. Each of these sequences has probability $p(A)^m p(B)^n$. By summing up these probabilities, the total probability of all sequences of a given length can be determined.

[1] N. J. Corron, J. N. Blakely, and M. T. Stahl, Chaos **20**, 023123 (2010).
[2] N. J. Corron and J. N. Blakely, Chaos **22**, 023113 (2012).
[3] T. Saito and H. Fujita, Electron. Commun. Jpn. 1 **64**, 9 (1981).
[4] T. Tsubone, K. Mitsubori, and T. Saito, in *Circuits and Systems, 1996. ISCAS '96, Connecting the World, 1996 IEEE International Symposium on Circuits and Systems*, Vol. 3 (IEEE, Washington, DC, 1996), pp. 257–260.
[5] T. Tsubone and T. Saijo, Circuits Syst. I: Fundamental Theory and Applications, IEEE Transactions on **45**, 172 (1998).
[6] A. N. Beal, J. P. Bailey, S. A. Hale, R. N. Dean, M. Hamilton, J. K. Tugnait, D. W. Hahs, and N. J. Corron, in *Proceedings 2012 Military Communications Conference, Orlando, FL, Oct. 29–Nov. 1, 2012* (IEEE, Washington, DC, 2012).
[7] B. A. M. Owens, N. J. Corron, M. T. Stahl, J. N. Blakely, and L. Illing, Chaos **23**, 033109 (2013).
[8] E. N. Lorenz, J. Atmos. Sci. **20**, 130 (1963).
[9] O. E. Rossler, Phys. Lett. A **57**, 397 (1976).
[10] N. J. Corron, J. N. Blakely, and M. T. Stahl, Chaos **22**, 029901 (2012).
[11] J. N. Blakely, D. W. Hahs, and N. J. Corron (unpublished).
[12] J. N. Blakely and N. J. Corron, in *Proceedings SPIE 8021, Radar Sensor Technology XV* (SPIE, Philadelphia, 2011), p. 80211H.
[13] N. J. Corron, M. T. Stahl, and J. N. Blakely, Chaos **23**, 023119 (2013).
[14] H.-P. Ren, M. S. Baptista, and C. Grebogi, Phys. Rev. Lett. **110**, 184101 (2013).
[15] V. Anishchenko, T. Vadivasova, G. Okrokvertskhov, and G. Strelkova, Physica A **325**, 199 (2003).
[16] A. Pikovsky, M. Rosenblum, and J. Kurths, *Synchronization: A Universal Concept in Nonlinear Sciences* (Cambridge University Press, Cambridge, 2001).
[17] V. Anishchenko, G. Okrokvertskhov, T. Vadivasova, and G. Strelkova, New J. Phys. **7**, 76 (2005).
[18] A. Csordas and P. Szepfalusy, Phys. Rev. A **38**, 2582 (1988).
[19] Z. Kaufmann, H. Lustfeld, and J. Bene, Phys. Rev. E **53**, 1416 (1996).
[20] J. Bene, Z. Kaufmann, and H. Lustfeld, J. Stat. Phys. **89**, 605 (1997).
[21] M. E. Yalcn, J. A. K. Suykens, and J. Vandewalle, IEEE Trans. Circ. Syst. I **51**, 1395 (2004).
[22] T. Addabbo, M. Alioto, A. Fort, S. Rocchi, and V. Vignoli, IEEE Trans. Circ. Syst. I **53**, 326 (2006).

[23] F.-Y. Lin and J.-M. Liu, IEEE J. Quantum Electronics **40**, 815 (2004).
[24] Z.-G. Shi, S. Qiao, K. S. Chen, W.-Z. Cui, W. Ma, T. Jiang, and L.-X. Ran, Prog. Elec. Res. **77**, 1 (2007).
[25] S. Tsekeridou, V. Solachidis, N. Nikolaidis, A. Nikolaidis, A. Tefas, and I. Pitas, Signal Process. **81**, 1273 (2001).
[26] B. Chirikov and D. Shepelyansky, Physica D **13**, 395 (1984).
[27] B. Dorizzi, B. Grammaticos, M. Le Berre, Y. Pomeau, E. Ressayre, and A. Tallet, Phys. Rev. A **35**, 328 (1987).
[28] D. Ruelle, J. Differential Geometry **25**, 99 (1987).
[29] F. Christiansen, G. Paladin, and H. H. Rugh, Phys. Rev. Lett. **65**, 2087 (1990).
[30] C. Liverani, Ann. Math. **142**, 239 (1995).
[31] D. Dolgopyat, Ann. Math. **147**, 357 (1998).
[32] N. Chernov, Ann. Math. **147**, 269 (1998).
[33] V. S. Anishchenko, T. E. Vadivasova, J. Kurths, G. A. Okrokvertskhov, and G. I. Strelkova, Phys. Rev. E **69**, 036215 (2004).
[34] M. Eisencraft, D. Kato, and L. Monteiro, Signal Process. **90**, 385 (2010).
[35] N. S. Tzannes, *Communication and Radar Systems* (Prentice-Hall, Upper Saddle River, 1985).
[36] G. M. Zaslavsky, *Chaos in Dynamical Systems* (Harwood Academic Publishers, Newark, 1985).